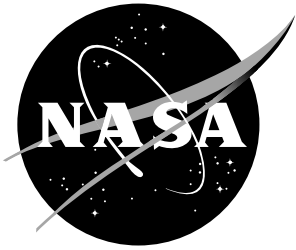


# Test Load Verification Through Strain Data Analysis

---

*V. Verderaime and F. Harrington*



# Test Load Verification Through Strain Data Analysis

---

*V. Verderaine and F. Harrington*  
*Marshall Space Flight Center • MSFC, Alabama*

## TABLE OF CONTENTS

	Page
I. INTRODUCTION .....	1
II. STRUCTURAL INTEGRITY .....	2
A. Verification .....	2
B. Binding Requirements.....	2
C. Mutating Boundary Loads .....	3
III. TEST RESPONSE ANALYSIS.....	4
A. Materials Modeling.....	4
B. Structural Modeling.....	6
C. Strain Profiles and Zone Limits.....	9
D. Normal Load and Moment Solutions .....	11
IV. LOADS PROGRAM.....	13
V. CONCLUSIONS .....	16
REFERENCES.....	17

## LIST OF ILLUSTRATIONS

Figure	Title	Page
1.	Applied load disposition at large boundary deformation.....	3
2.	Uniaxial tensile properties of polycrystalline materials.....	5
3.	Combined bending and normal loading element .....	6
4.	Combined bending and normal tension strains and stresses along the thickness.....	7
5.	Strain profiles over element cross section defined by measured surface strains.....	9
6.	Combined normal and bending stress and strain projections.....	10
7.	Program sample output.....	15
8.	Strain distributions.....	15
9.	Stress distributions.....	15

## NOMENCLATURE

$N$	normal load, kips
$M$	moment, kip-inches
$F$	material strength, ksi
$C$	cross-sectional limits, inches
$H$	element thickness, inches
$w$	element width, inches
$y$	vertical axis
$x$	longitudinal axis
$E$	elastic modulus, ksi
$n$	strain-hardened exponent
$K$	strength coefficient, ksi
$\sigma$	normal stress, ksi
$\varepsilon$	normal strain
$\theta$	slope, degrees

### Subscripts

$ty$	tensile yield
$tu$	tensile ultimate
$cy$	compression yield
$e$	elastic
$p$	inelastic
$N$	normal
$M$	bending
$o$	elastic limit
$y$	vertical axis
1	minimum strain data
2	maximum strain data
$k$	zone number

## TECHNICAL PAPER

# TEST LOAD VERIFICATION THROUGH STRAIN DATA ANALYSIS

## I. INTRODUCTION

Increasing demands for more reliable and affordable access to space is promoting leaner and more innovative structural designs that invoke more reliance on experimental verification. This compelling shift should raise concerns on how well verification tests are implemented. A brief review of verification requirements and methods revealed a potential test load transfer error at very flexible structural boundaries. A technique for identifying and analyzing applied load diversions is suggested.

Least initial and recurring costs of high-performance structures are achieved through select combinations of new materials and manufacturing processes, advanced modeling technologies, limited arbitrary design factors, etc. These performance cost improvements are balanced with the cost of reliability design that is reflected in structural weight increase leading to recurring increased delivery cost. Proof of this delicate design balance between performance and reliability depends, first on performance verification through structural response testing, and then on verification of design environments through field and flight testing. Success of these verifications is further predicated on the true transfer of environments onto the structure.

Assemblies of large, high-performance structures are inherently very flexible. And though structural boundary rotations and deflections at externally applied loads are not significant to response verification up to operational limits, successively larger boundary loads and distortions approaching rupture may unknowingly compromise the ultimate safety criteria with serious consequences. Improperly transmitted verification loads may reject a perfectly adequate design or accept a submarginal one. Both lead to costly redesign, with the latter case being discovered after flight test, which is at a worse quality level phase.<sup>1</sup>

A technique was developed to measure and analyze the variance of the transmitted verification loading through the most commonly encountered structural element. A one-dimensional bending and normal loading element was selected for developing strain response models throughout the elastic and inelastic ranges. The technique uses strain data from two back-to-back surface-mounted gauges to analyze, define, and monitor the induced moment and plane force through progressive material changes from total-elastic to total-inelastic within the cross section. Measured boundary applied loads and calculated induced loads from strain data are compared. Deviations caused from excessive local deformation and deflections are identified by the consecutively changing ratios of moment-to-axial load. Resulting deviations may be analyzed and correlated for compliance with safety criteria.

The analysis is simplified through the application of an elastic-inelastic two-parameter material model. The analytical approach is also applicable with plastic theory,<sup>2</sup> or tabulated inelastic properties. The analysis is programmed in basic for convenience and expediency. Inplane and transverse shear load deviations may also be analyzed through similar instrumentation and analysis. The technique can be extended to multiaxial stresses and to other strength-of-materials elements as necessary.

## **II. STRUCTURAL INTEGRITY**

All such current design processes as customer's voice, total quality management, concurrent engineering, etc., stem from the core design philosophy on integrity. Tenets of design integrity are that it must perform well under a liberal range of environments, over a specified life, and reliably. Challenges are to reduce these basics into engineering specifications, design to them, and determine the extent and methods for verifying them with least cost. Genuine incentives for producing high structural integrity products are to experiment in quality test methods. Selection of a structural verification option, its conduct, interpretations, and design feedback are some of the most important development functions in fixing manufacturing processes, operations reliability, and cost characteristics into a product's total life cycle. Verification criteria should be updated and satisfied through refined design analyses, similarity with successfully operating structures, or experimental testing. Experimental testing is often the most expensive and difficult to satisfy and is the focus of this quality function.

### **A. Verification**

Commonly stated requirements for experimental testing are to verify design assumptions, expose incomplete analysis, avoid sneak phenomena, affirm critical-failure and postfailure modes, reveal unique response characteristics, verify math model responses and margins, and develop inspection procedures. Experimental testing may provide insights to redundant failure modes and to foolproof concepts that need to be introduced in critical manufactured parts, assemblies, joints, seals, and changeout interfaces. Tests might also identify operational bottlenecks ensuing when quality targets are set at higher levels than previously experienced and levels are difficult to achieve.

Of these requirements, safety margin verification is the prime concept driver. Tests may be performed to failure or to no-failure. A no-fail test provides limited margin experience, no matter how successfully it operates thereafter. It does provide multiple opportunities to verify, on a single article, predicted responses in many high-stress regions subjected to different operational environments. Test and field or flight tests are no-fail types of tests requiring no additional hardware costs.

However, it should be recognized that most structural tests provide only limited surface data that must be correlated with design math models to completely verify yield and fracture stresses. Tests whose boundaries and operational environments are difficult to simulate may also yield results that are difficult to interpret. Therefore, components and critical structural regions of no-fail test articles should be off-line tested to fracture, provided binding loading conditions are credibly simulated and propagated through the entire loading range to fracture. Fractured tests may be further evaluated through metallurgical features of parted surfaces.

### **B. Binding Requirements**

Going into a structural static test, the predicted design variables are the applied boundary loads representing strategic operational environments, associated uncertainties, mechanical response of structural elements, and material properties and limits. These predictions are verified by their combined effects defined by the ratio of material resistive properties and the applied boundary load. This ratio specifies the prevailing deterministic factor of safety,<sup>3</sup> which is a binding verification criterion, and deserves some evaluation.

NASA's safety criteria on polycrystalline structures are a verified 1.0 factor on yield and a 1.4 factor on ultimate. Both factors propose a few interesting realities. If the inception of plastic flow on a test article could be experimentally detected, the measured load producing it would suitably establish the yield safety factor. However, plastic deformation<sup>4</sup> starts in different locations, numbers, and intensities, and it is difficult to detect and determine where and how much deformation progressed until large enough parts have been affected at the strain sensors. This phenomenon explains why different gauge lengths in tensile tests provide different elastic limits, why yield coefficients of variation are higher than strength variations, and why it is more difficult to detect the limit in brittle materials. Hence, an arbitrarily selected standard for defining the yield point is the intersection of a line parallel to and offset by 0.2 percent from the elastic stress-strain slope. For consistency, should a similar offset be applied to the load-strain slope attained from verification test data?

Structures are often subjected to a loading history that may exceed the elastic limit and raise the yield point for subsequent loading. The plastic flow property of metals is important in economic manufacturing processes such as rolling, forging, drawing, extruding, stamping, bending, riveting, and spinning. This inelastic property also allows material to flow and redistribute concentrated peak stresses optimally and permanently, and then retain the full elastic strength for repeated cycles. Under these and similar initial processes, the material is transformed, and the raised yield point may obscure the operational strain limit verification and may unexpectedly reduce endurance predictions and contingency margin to fracture.

Conversely, the onset and measured load at fracture in the loading process can be clearly established, but the load transferred at the boundary and its propagation to critical regions may be uniquely and unforeseeable conditioned by larger plastic deformation preceding fracture. It was this potential transfer behavior that lead to the investigation of shifting response loads and composition under increasingly applied boundary loading.

### C. Mutating Boundary Loads

Increasing verification loads applied at test article boundaries produce progressively larger deformations beyond the inelastic range which may distort their transmission. To sample this phenomenon, the slope and deflection were calculated at the concentrated load on the free-end of the cantilevered beam (fig. 1). The hypothetical aluminum beam is 10 inches long and a quarter-inch uniform thickness. Deflections and slopes are shown for the yield and ultimate strain limits calculated<sup>5</sup> at the fixed-end. The tangent of the free boundary slope is a measure of the consecutively applied load decomposing from bending to bending-axial load ratio. This ratio varies with the slope along the beam. Though the vertical scale in figure 1 is exaggerated, the slopes and displacements at the free end are relative.

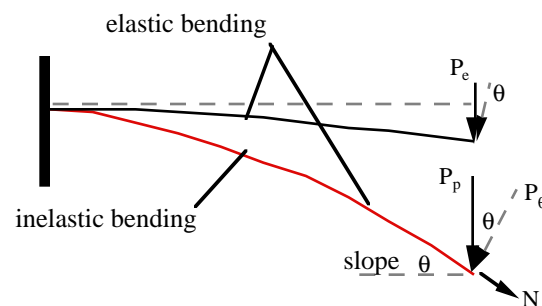


Figure 1. Applied load disposition at large boundary deformation.

Because the yield strain at the fixed-end is relatively small, the predicted free-end elastic deflection and slope are correspondingly small, and the variation between applied and transmitted loads is the tangent of  $5^\circ$ , which is negligible. The ultimate load to fracture is twice the yield load, and the resulting ultimate strain at the fixed-end is an order-of-magnitude larger than the yield. At ultimate loading, about half the beam near the fixed-end is deflecting inelastically, and the free-end half is deflecting elastically at a lower rate. The combined deflections predict an  $18^\circ$  slope resulting in a 33-percent bending-to-axial load ratio. The adversity of this ratio to the verification criteria is dependent on how these components feed into and intensify critically stressed regions and how they may change the failure mode.

It is conceivable that this phenomenon occurring with some other material, type element, and boundary loading may allow a marginal structure to pass the static test criteria because of a more benign transmitted load deviation, or to fail an unsuspected safe article. Consider the welded region on a shell designed to sustain only normal tensile strain. If a large, unintentional bending deformation is introduced by the verification load through the inelastic region, the shell will prematurely fail at the weld. Bending causes the weld material having the lowest elastic limit to hinge and assume a disproportionate share of distortion. The small weld width limits the extent of distortion to failure. The combination of the small weld width and lowest elastic limit causes the weld material to yield first and progressively distort most to fracture. This is a metallurgical discontinuity stress failure. Other discontinuity stress regions may be identified by abrupt changes in loads, geometry, and temperature which induce multiaxial loads that may be adversely intensified by distorted boundary load transmission.

The cantilevered beam, the welded shell, and many other elements experiencing distorted boundary loads are most often noted to include inplane normal and bending components. Auspiciously, these inplane normal and bending loads are readily derivable from two opposite mounted strain gauges. Their experimental applications include verification of applied test load on scaled test article and off-line structural component, tracking response loads deviations during test loading beyond the elastic limit, field, and flight test environment verification, etc. Such a technique was developed on a one-dimensional stress element because of its wide application and its simplistic illustration.

### **III. TEST RESPONSE ANALYSIS**

Analysis of the applied load deviation to fracture is based on selecting a simple elastic-inelastic material model, identifying and defining structural variables, and developing a technique for bounding and zoning stress-strain distributions over the cross section through two surface-mounted strain gauge readings.

#### **A. Materials Modeling**

Approximately 90 percent of primary aerostructural weight is composed of polycrystalline materials such as high specific strength steels and aluminums. Most common material structural properties required for a one-dimensional stress analysis are those defined by the simplest one-dimensional test, the uniaxial tension test. Figure 2 typifies the stress-strain relationships and the elastic and inelastic transformation limits of a polycrystalline material derived from such a test.

The segment  $O-\sigma_o$  is the linear elastic region of the material which is governed by the resilience between atoms within a crystal. When an applied load is relieved, the deformation will recover to its original position, “O.” This linear stress-strain relationship defines Hooke’s law, and the limit is reached when atoms permanently displace along cleavage planes to new crystal lattice sites in plastic flow. The 2-percent offset defines the yield point previously discussed.

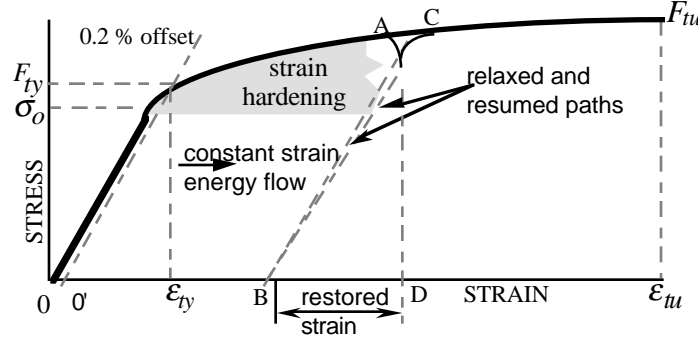


Figure 2. Uniaxial tensile properties of polycrystalline materials.

The segment from the elastic limit,  $\sigma_o$ , up to the ultimate stress,  $F_{tu}$ , is the inelastic (or ductile) region of the material consisting of elastic stress and plastic flow. The ratio of elastic stress and plastic flow defines the inelastic slope, and their change rate characterizes the nonlinear property of the material to fracture. When loaded to point “A” and relaxed, the strain decreases elastically to point “B.” The material will have restored the elastic strain B-D, and will have permanently deformed with a plastic strain of O’-B. Upon reloading, the unit load traces a hysteresis loop as it approaches point “C” near point “A” from which it was unloaded, and then resumes the stress-strain relationship as it had not relaxed.

Modeling elastic-inelastic behavior could be very difficult unless idealized into the simplest mathematical expressions within the physical phenomena of the material and its application. Some finite element method codes tabulate the nonlinear material coordinates of figure 2 and compute the linear strength of materials behavior with the inelastic property in a piece-wise-linear technique. The analytical approach used in this study modeled the total range of uniaxial stress-strain relationship by the two parameter power expression,

$$\sigma = K \epsilon^n , \quad (1)$$

where “ $n$ ” is the strain-hardening exponent and “ $K$ ” is the strength coefficient of the inelastic region. The exponent  $n = 0$  defines a perfectly plastic solid. The linear elastic region is defined by  $n = 1.0$  and the Young’s modulus,

$$E = \frac{F_{ty}}{\epsilon_{ty}} . \quad (2)$$

Wherever subsequent formulations are expressed with nonlinear parameters, they may be converted to elastic expressions through the substitution of  $n = 1$  and  $K = E$ .

The inelastic parameters of equation (1) are curve-fitted at the extremes of the nonlinear segment in figure 2. The strain-hardening exponent is calculated from,

$$n = \frac{\log (F_{tu}/F_{ty})}{\log (\epsilon_{tu}/\epsilon_{ty})} , \quad (3)$$

and the strength coefficient is,

$$K = \frac{F_{ty}}{\epsilon_{ty}^n} . \quad (4)$$

Material stress-strain properties are customarily assumed to be symmetrical in tension and compression. It must be noted, though, that for structures that are work hardened through manufacturing shaping, milling, and other processes and are not thereafter annealed, the yield parameters in equations (3) and (4) must be derived with the reloaded values noted by the points B and C on figure 2.

## B. Structural Modeling

A rectangular cross-section element illustrated in figure 3 was selected because it represents most structural components and regions as in beams, plates, and shells. It is also the simplest cross section to demonstrate the technique for characterizing the elastic and inelastic stress and strain distributions, and for determining the applied loads transfer. Bending and inplane normal loadings are the most commonly measured components on this type of structure with back-to-back strain gauges, and they often may be of sufficient sample to verify the load transmission of a more complex system.

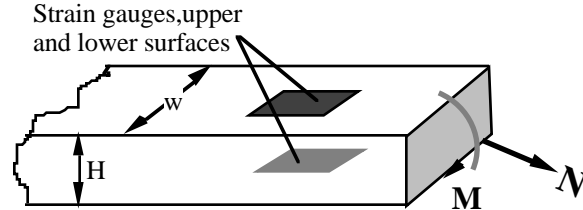


Figure 3. Combined bending and normal loading element.

The normal load,  $N$ , is constant along the thickness,  $H$ , from which the induced normal stress,

$$\sigma_N = \frac{N}{wH} , \quad (5)$$

and strain,

$$\epsilon_N = \left[ \frac{N}{K w H} \right]^{\frac{1}{n}} , \quad (6)$$

are uniformly distributed over the elastic and inelastic range. The elastic bending stress and strain are linearly varying along the thickness. Because cross-section planes are seen to remain plane after elastic and plastic bending, the inelastic bending strain also varies linearly along the thickness, but the stress varies nonlinearly with equation (1). The stresses and strains at the extreme (surface) fibers for elastic and inelastic bending are thus given<sup>5</sup> by,

$$\sigma_M = \pm \frac{2(n+2)M}{H^2}, \quad (7)$$

and

$$\varepsilon_M = \pm \left[ \frac{2(n+2)M}{KH^2} \right]^{\frac{1}{n}}, \quad (8)$$

respectively.

Because inelastic bending stress is nonlinear, it cannot be directly superimposed on the normal tension stress of equation (5), nor is the bending neutral axis expected to coincide with the cross-section centroid. However, an interacting model may be formulated by noting that the normal strain is uniformly linear along the cross section and the bending strain is linearly varying along the thickness. Since both axial strains are linear, they may be algebraically added as shown in figure 4(a). These combined strains are measured at the surfaces as  $\varepsilon_2$  and  $\varepsilon_1$ . Figure 4(b) illustrates the nonlinear bending stress distribution derived from the strain distribution using equation (1).

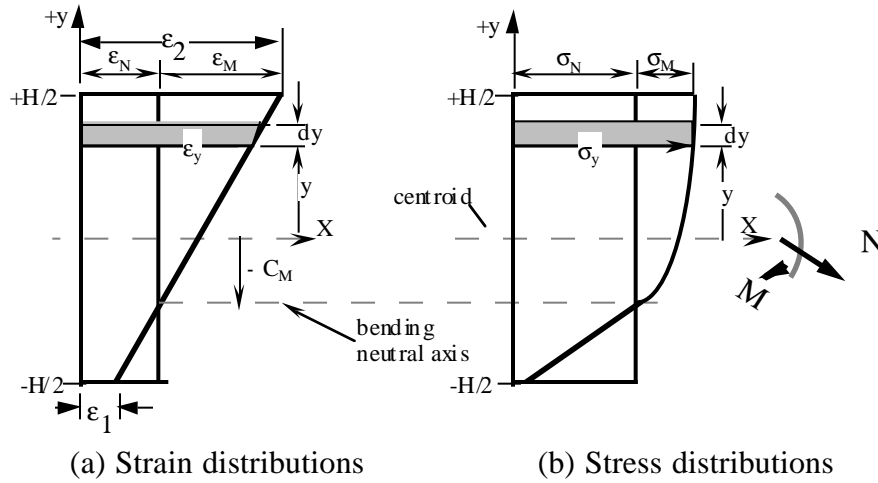


Figure 4. Combined bending and normal tension strains and stresses along the thickness.

Since the elastic as well as the inelastic normal tension and bending strains are mutually linear, the combined strain distribution in figure 4(a) is an appropriate diagram to derive variables and relationships required to determine the verification normal and bending loads. Of the two back-to-back surfaces measured strains,  $\varepsilon_2 > \varepsilon_1$  will be assumed throughout the study to simplify elastic and inelastic zone notations. When  $\varepsilon_2 < \varepsilon_{ty}$ , the combined strain distributions over the cross section are all in one elastic zone, and, when  $\varepsilon_1 > \varepsilon_{ty}$ , the distributions are all one inelastic zone. The objective is now to define the elastic-inelastic zone boundaries for all other measured strain combinations and to calculate their contributions to the resulting normal and bending loads.

The net strain from any midplane  $y$ -distance along the element thickness in figure 4(a) is defined by the proportionality,

$$\frac{\varepsilon_y - \varepsilon_1}{\varepsilon_2 - \varepsilon_1} = \frac{\frac{H}{2} + y}{H} ,$$

or

$$\varepsilon_y = \gamma(0.5H + y) + \varepsilon_1 , \quad (9)$$

and

$$y = \frac{1}{\gamma} (\varepsilon_y - \varepsilon_1) - 0.5H . \quad (10)$$

The bending strain slope is,

$$\gamma = \frac{\varepsilon_2 - \varepsilon_1}{H} . \quad (11)$$

The incremental normal load along the cross-section thickness is the product of the induced stress and unit area,

$$dN = w \sigma_y dy = wK(\varepsilon_y)^n dy . \quad (13)$$

Substituting equation (9) for the strain and integrating, all zone normal loads may be calculated from,

$$N_k = \frac{wK\gamma^n}{n+1} \left[ \frac{H}{2} + \frac{\varepsilon_1}{\gamma} + y \right]^{n+1} \Big|_{C_b}^{C_a} , \quad (14)$$

where  $C_a > y > C_b$  are the integration limits of a zone. A zone is bound along the y-axis by the surface measured strains,  $\varepsilon_1$  and  $\varepsilon_2$ , or by the material limit changes noted by  $\varepsilon_{ty}$  and  $\varepsilon_{cy}$ . Substituting the appropriate pair of boundary strains into equation (10),

$$C_{a,b} = \frac{1}{\gamma} (\varepsilon_{a,b} - \varepsilon_1) - \frac{H}{2} , \quad (15)$$

provides the upper and lower integration limits of each zone. The yield strain may be tension or compression, where  $\varepsilon_{cy} = -\varepsilon_{ty}$  is assumed for a symmetrical material. The normal load across the thickness is the sum of all the zone normal loads,

$$N = \sum N_k . \quad (16)$$

Bending strain along the thickness is given by  $\varepsilon_{My} = \varepsilon_y - \varepsilon_N$ , and the neutral bending axis is defined by a zero bending strain ( $\varepsilon_{My} = 0$ ). Substituting  $\varepsilon_y = \varepsilon_N$  into equation (10), the neutral bending axis is,

$$C_M = \frac{1}{\gamma} (\varepsilon_N - \varepsilon_1) - 0.5H , \quad (17)$$

where the normal strain,  $\varepsilon_N$ , across the thickness is determined by substituting equation (16) into equation (6). Using equations (13) and (17), the incremental moment about the neutral axis is,

$$dM = w \sigma_y (y - C_M) dy = wK(\varepsilon_y)^n (y - C_M) dy . \quad (18)$$

By substituting equations (9) and (17) into equation (18) and integrating, a zone moment about the neutral axis is calculated from,

$$M_k = wK\gamma \left[ \frac{H}{2} + \frac{\epsilon_1}{\gamma} + y \right]^{n+1} \left\{ \frac{\frac{H}{2} + \frac{\epsilon_1}{\gamma} + y}{n+2} - \frac{\frac{H}{2} + \frac{\epsilon_1}{\gamma} + C_M}{n+1} \right\} \Big|_{C_b}^{C_a} . \quad (19)$$

The moment about the thickness is the sum of all the zone moments,

$$M = \sum M_k . \quad (20)$$

A unit width,  $w = 1$ , is assumed for plates and shells from which normal loads and bending moments are defined by kips per inch and kip-inch per inch units, respectively. Using the strain distribution expression of equation (9), the stress distribution along each zone is given by,

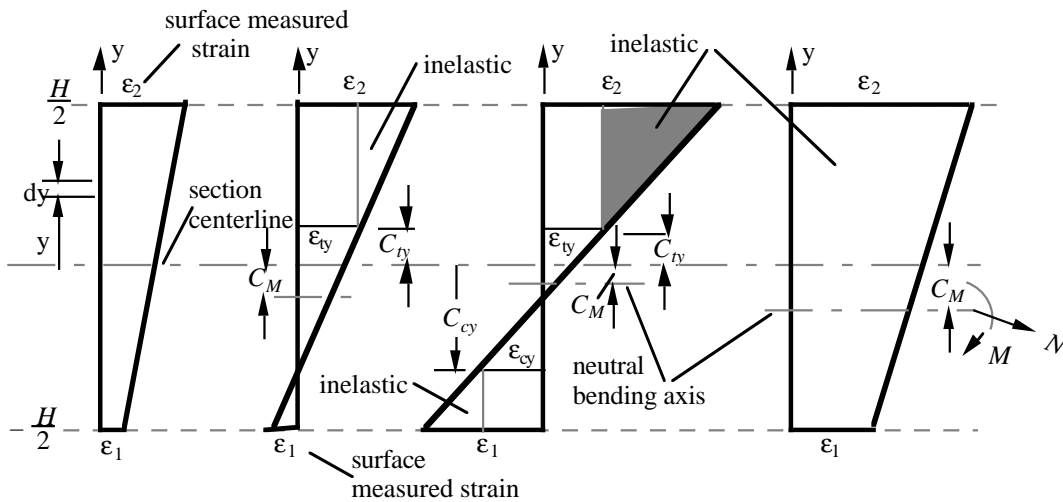
$$\sigma_y = K [ABS(\epsilon_y)]^n SGN(\epsilon_y) . \quad (21)$$

Expressions in absolute form allow raising strains to odd powers.  $SGN()$  is the signum function, which reestablishes the sign of the expression. If its sign is positive, then the function equals +1 and the strain is positive. If the function equals -1, the strain is negative.

These models, associated variables, and related integration limits are the means for calculating the desired normal and bending loads from any combination of elastic-plastic strain profile.

### C. Strain Profiles and Zone Limits

As the induced normal and bending loads in figure 3 increase, the strain distribution over the element cross section progresses from totally elastic to totally inelastic in four possible profiles and in a sequence dependent on the loading schedule. Given the values of the two measured strains,  $\epsilon_1$  and  $\epsilon_2$ , the related profile is directly selected, and the zones and integration limits are decided as shown in figure 5.



- (I)  $\epsilon_{cy} < \epsilon_1 < \epsilon_2 < \epsilon_{ty}$     (II)  $\epsilon_{cy} < \epsilon_1 < \epsilon_{ty} < \epsilon_2$     (III)  $\epsilon_1 < \epsilon_{cy} < \epsilon_{ty} < \epsilon_2$     (IV)  $\epsilon_{ty} < \epsilon_1 < \epsilon_2$

Figure 5. Strain profiles over element cross section defined by measured surface strains.

In general, the measured strain  $\epsilon_2$  is here assumed to be always greater than  $\epsilon_1$ , and change in material properties is understood to be a change from elastic-to-inelastic strain noted by the yield strain and vice versa. Therefore, if  $\epsilon_2$  is less than tension yield,  $\epsilon_{ty}$ , and  $\epsilon_1$  is greater than compression yield,  $\epsilon_{cy}$ , then no change of properties transpires and the strain profile is a single elastic zone as shown in profile (I) (fig. 5). A two-zone profile (II) is established when a material change occurs in which the yield strain value falls between the two surface-measured strains. A double change in materials (tension and compression yield) occurring between the measured strains distinguishes a three-zone profile (III). When both measured strains exceed the tension yield point, the profile (IV) is a single inelastic zone.

Perhaps a more visual appreciation of how the normal and bending stress and strain distributions interact may be realized through their orthographic projection with the material properties shown in figure 6. Figures 6(a) and 6(b) are the stress and strain distribution diagrams, respectively, over the element rectangular cross section. Figure 6(c) is the material tension stress-strain relationship through the elastic and inelastic range. Projecting the two surface strains,  $\epsilon_1$  and  $\epsilon_2$ , from figure 6(b) up to the material diagram 6(c), locates the corresponding stresses which are then projected and intersected on the stress diagram 6(b). Projecting the yield point from the material diagram 6(c) onto the stress and strain diagrams establishes the inelastic zones (shaded area) on the stress and strain diagrams and as imposed on the structural element.

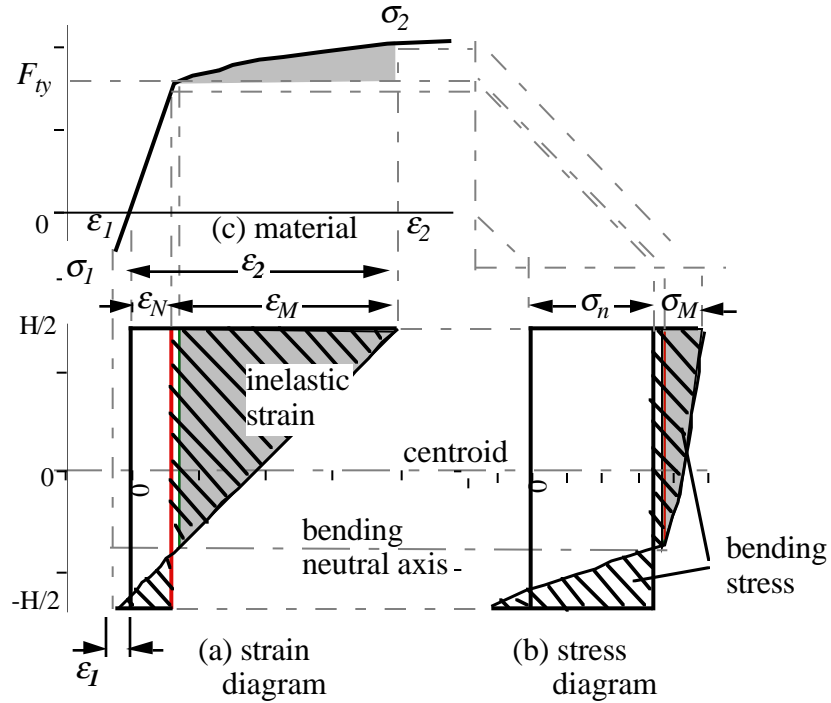


Figure 6. Combined normal and bending stress and strain projections.

Projecting the normal strain distribution from figure 6(a) onto the material diagram determines the corresponding stress, and that stress defines the uniform stress distribution in the stress diagram (fig. 6(b)). The intersection of the normal and bending strain distributions locates the bending neutral axis which is extended into the stress diagram. Projecting bending strains from figure 6(a) to 6(c) and to 6(b), and intersecting associated stresses from 6(c) with 6(a) onto 6(c) develops the nonlinear bending stress distribution (cross hatched area) in figure 6(b). The bending stress distribution curve over the thickness in figure 6(b) resembles the elastic-inelastic stress-strain

profile of figure 6(c). Also note that the bending stress area above the bending neutral axis is equal and opposite to that below the bending axis, which satisfies the moment equilibrium.

Back-to-back strain gauges are sometimes used to isolate pure normal strains from bending strains by averaging the two strain gauge output. But beyond the elastic limit, this rule is demonstrated to be not valid, and there is no easy method for isolating the normal strain from combined strain data except through an inelastic math model. Since distinct changes in material properties and load paths evolve beyond the elastic limit, analysts are deprived of these insights without an expedient and available to identify and define them.

### D. Normal Load and Moment Solutions

The induced combined normal and bending moment loads in each strain profile may be resolved through a straightforward analytical routine summarized as follows:

- From the pair of surface measured strains, identify its strain profile in figure 5 through number of zones and related boundary strains
- Using strains at zone boundaries in the selected figure 5 profile, define the integration limits  $C_{a,b}$  for each zone from equation (15)
- Substitute integration limits from equation (15) into equation (14) and solve for the normal load  $N_{I,k}$  of each zone in the profile
- Normal loads from all zones determined from equation (14) are summed in equation (16) to obtain the net total normal load  $N$  of the profile
- Substitute total normal load of equation (16) into equation (6) to obtain the profile normal strain,  $\epsilon_N$
- Locate the bending neutral axis  $C_M$  using the total normal strain from equation (6) in equation (17)
- Using equation (19), determine the bending moment  $M_{I,k}$  in each zone about the neutral bending axis of equation (17)
- Sum the moments in the profile as in equation (20)
- Plot strain distribution  $\epsilon_y$  over the thickness using equation (9)
- Plot stress distribution  $\sigma_y$  over the thickness using equation (21).

This direct, though laborious, routine suggests the need for a simple computer code. Consequently, only those expressions unique to a zone and profile are developed in the sequence as necessary to verify the program.

**Profile (IV)**, ( $\epsilon_{ty} < \epsilon_1 < \epsilon_2$ ), is a single inelastic zone with integration limits of  $C_a = H/2$  and  $C_b = -H/2$  as calculated from equation (15) using boundary strains  $\epsilon_2$  and  $\epsilon_1$ , respectively. The profile total normal load and bending moment are,

$$N_{IV} = \frac{wK}{(n+1)\gamma} [(\varepsilon_2)^{n+1} - (\varepsilon_1)^{n+1}] \quad , \quad (23)$$

and

$$M_{IV} = \frac{wK}{\gamma^2} \left[ \frac{(\varepsilon_2)^{n+2} - (\varepsilon_1)^{n+2}}{n+2} - \frac{(\varepsilon_2)^{n+1} - (\varepsilon_1)^{n+1}}{n+1} \left( \frac{\varepsilon_1 + \varepsilon_2}{2} + \gamma C_M \right) \right] \quad , \quad (24)$$

respectively, where the neutral bending axis from equation (17) is,

$$C_M = \frac{1}{\gamma} \left( \left[ \frac{(\varepsilon_2)^{n+1} - (\varepsilon_1)^{n+1}}{(n+1)H\gamma} \right]^{\frac{1}{n}} - \varepsilon_1 \right) - \frac{H}{2} \quad . \quad (25)$$

**Profile (I)**, ( $\varepsilon_{cy} < \varepsilon_1 < \varepsilon_2 < \varepsilon_{ty}$ ), is a single elastic zone having similar integration limits as profile (IV). Substituting the elastic properties,  $K = E$  and  $n = 1$ , into equations (23), (24), and (25) produces the elastic normal load, bending moment and bending axis

$$N_I = \frac{wE}{2} (\varepsilon_2 + \varepsilon_1) \quad , \quad (26)$$

$$M_I = \frac{wEH^2}{12} (\varepsilon_2 - \varepsilon_1) \quad , \quad (27)$$

$$C_M = 0 \quad , \quad (28)$$

respectively.

**Profile (II)**, ( $\varepsilon_{cy} < \varepsilon_1 < \varepsilon_{ty} < \varepsilon_2$ ), consists of two zones. The two pairs of integration limits are  $C_a = H/2$ ,  $C_b = C_{ty}$ , and  $C_a = C_{ty}$ ,  $C_b = -H/2$  where,

$$C_{ty} = \frac{1}{\gamma} (\varepsilon_{ty} - \varepsilon_1) - \frac{H}{2} \quad . \quad (29)$$

The normal loads for the two zones are,

$$N_{II,1} = \frac{wK}{(n+1)\gamma} [(\varepsilon_2)^{n+1} - (\varepsilon_{ty})^{n+1}] \quad , \quad (30)$$

$$N_{II,2} = \frac{wE}{2\gamma} [(\varepsilon_{ty})^2 - (\varepsilon_1)^2] \quad . \quad (31)$$

Bending moments are,

$$M_{II,1} = \frac{wK}{\gamma^2} \left\{ \frac{(\varepsilon_2)^{n+2} - (\varepsilon_{ty})^{n+2}}{n+2} - \frac{(\varepsilon_2)^{n+1} - (\varepsilon_{ty})^{n+1}}{n+1} \left[ \frac{\varepsilon_1 + \varepsilon_2}{2} + \gamma C_M \right] \right\} \quad , \quad (32)$$

and

$$M_{II,2} = \frac{wE}{\gamma^2} \left\{ \frac{(\epsilon_{ty})^3 - (\epsilon_1)^3}{3} - \frac{(\epsilon_{ty})^2 - (\epsilon_1)^2}{2} \left[ \frac{\epsilon_1 + \epsilon_2}{2} + \gamma C_M \right] \right\} . \quad (33)$$

**Profile (III)**,  $(\epsilon_1 < \epsilon_{cy} < \epsilon_{ty} < \epsilon_2)$ , includes three zones having three pairs of integration limits:  $C_a = H/2$ ,  $C_b = C_{ty}$ ;  $C_a = C_{ty}$ ,  $C_b = C_{cy}$ ;  $C_a = C_{cy}$ ,  $C_b = -H/2$ . The normal loads are ,

$$N_{III,1} = N_{II,1} , \quad (34)$$

$$N_{III,2} = \frac{wE}{2\gamma} (\epsilon_{ty}^2 - \epsilon_{cy}^2) , \quad (35)$$

and

$$N_{III,3} = \frac{wK}{(n+1)\gamma} \left[ (ABS(-\epsilon_{ty}))^{n+1} - (ABS(\epsilon_1))^{n+1} \right] . \quad (36)$$

The bending moments are,

$$M_{III,1} = \frac{wK}{\gamma^2} \left\{ \frac{(\epsilon_2)^{n+2} - (\epsilon_{ty})^{n+2}}{n+2} - \frac{(\epsilon_2)^{n+1} - (\epsilon_{ty})^{n+1}}{n+1} \left[ \frac{\epsilon_1 + \epsilon_2}{2} + \gamma C_M \right] \right\} , \quad (37)$$

$$M_{III,2} = \frac{wE}{\gamma^2} \left\{ \frac{2\epsilon_{ty}^3}{3} - \epsilon_{ty}^2 \left[ \frac{\epsilon_1 + \epsilon_2}{2} + \gamma C_M \right] \right\} , \quad (38)$$

$$M_{III,3} = \frac{wK}{\gamma^2} \left\{ \frac{(ABS(-\epsilon_{ty}))^{n+2} - (ABS(\epsilon_1))^{n+2}}{n+2} - \frac{(ABS(-\epsilon_{ty}))^{n+1} - (ABS(\epsilon_1))^{n+1}}{n+1} \left[ \frac{\epsilon_1 + \epsilon_2}{2} + \gamma C_M \right] \right\} . \quad (39)$$

#### IV. LOADS PROGRAM

Though programs are usually delegated to the appendix, all math models and expressions developed above are appropriately synthesized here. Normal load and bending moment solutions derived from two surface-measured strains include the four strain profiles illustrated in figure 5. Code is in Microsoft Quick Basic™ for application on most small computers.

Profile (III), having the most zones, was solved and programmed as outlined in the preceding section. Other profiles, having less zones, were adapted by resetting limits according to their zone boundary values and positions in the strain diagrams and applying them to their appropriate zones.

'NORMAL/BENDING LOADS FROM STRAIN DATA  
'NMLFSD, Microsoft Quick Basic™

' MATERIAL PROPERTIES  
INPUT "ELASTIC MODULUS E=";ELM  
INPUT "YIELD STRESS Fty=";FTY  
INPUT "MAX STRESS Ftu=";FTU  
INPUT "STRAIN @ MAX STRESS Etu=";ETU  
  
ETY=FTY/ELM

PRINT "TENSION YIELD STRAIN";ETY  
ECY=-ETY  
SHE=LOG(FTU/FTY)/LOG(ETU/ETY)  
PRINT "STRAIN HARDENING EXPO. n=";SHE  
K=FTY/(ETY^SHE)  
PRINT "STRENGTH COEF K=";K  
K0=K  
SHE0=SHE  
ECY0=ECY  
ETY0=ETY

```

"TEST DATA
INPUT "RECT BAR THICKNESS H=";H
INPUT "BAR WIDTH w=";W

10 INPUT "TEST MAX STRAIN E2=";E2
INPUT "TEST MIN STRAIN E1=";E1
IF E2<E1 THEN
PRINT "MAX STRAIN < MIN STRAIN"
GOTO 10
END IF
IF E2=E1 THEN E1=0.975
SLOP=(E2-E1)/H

PRO=3
'USING PROFILE (III) (E1<ECY<ETY<E2)
IF ECY<E1 AND E1<ETY AND ETY<E2 THEN
ECY=E1:PRO=2
ELSEIF ETY<E1 AND E1<E2 THEN
ECY=E1:ETY=E1:PRO=4
ELSEIF E2<ETY AND ECY<E1 THEN
K=ELM :SHE=1:ECY=E1:ETY=E2:PRO=1
END IF

NIII1=W*K*(E2^(SHE+1)-ETY^(SHE+1))/(SLOP*(SHE+1))
NIII2=W*ELM*((ETY^2)-(ECY^2))/(2*SLOP)
NIII3=(ABS(ECY))^(SHE+1)-(ABS(E1))^(SHE+1)
NIII3=NIII3*W*K/(SLOP*(SHE+1))
NIIIT=NIII1+NIII2+NIII3
PRINT "TOTAL AXIAL LOAD N=";NIIIT
SNIII=NIIIT/W/H
PRINT "AXIAL LOAD STRESS SN=";SNIII

IF SNIII<FTY THEN
ENIII=SNIII/ELM
ELSE
ENIII=(SNIII/K)^(1/SHE)
END IF
PRINT "AXIAL LOAD STRAIN EN=";ENIII
EMMIII=E2-ENIII
PRINT "MAX BENDING STRAIN EM=";EMMIII

CMIII=(ENIII-E1)/SLOP-H/2
PRINT "BENDING NEUTRAL AXIS CM=";CMIII

MIII1=-((E2^(SHE+1))-(ETY^(SHE+1)))/(SHE+1)
MIII1=MIII1*((E1+E2)/2+CMIII*SLOP)
MIII1=MIII1+((E2^(SHE+2))-(ETY^(SHE+2)))/(SHE+2)
MIII1=MIII1*W*K/(SLOP^2)
MIII2=-((ETY^2)-(E1^2))*((E1+E2)/2+CMIII*SLOP)/2
MIII2=MIII2+((ETY^3)-(E1^3))/3
MIII2=MIII2*W*ELM/(SLOP^2)
MIII3=-((ABS(ECY))^(SHE+1)-
(ABS(E1))^(SHE+1))/(SHE+1)
MIII3=MIII3*((E1+E2)/2+CMIII*SLOP)
MIII3=MIII3+((ABS(ECY))^(SHE+2)-
(ABS(E1))^(SHE+2))/(SHE+2)
MIII3=MIII3*W*K/(SLOP^2)
MIIIT=MIII1+MIII2+MIII3
PRINT "BENDING MOMENT M=";MIIIT

RIII=MIIIT/NIIIT
PRINT "MOMENT/AXIAL LOAD RATIO R=";RIII

```

PrintScreen 0,0,0

LIMITS

```

CTY=(ETY-E1)/SLOP-H/2
CCY=(ECY-E1)/SLOP-H/2
ETYA=FTY/ELM

```

' STRESS & STRAIN DISTRIBUTIONS  
OPEN "CLIP:" FOR OUTPUT AS #2

PRINT "PROFILE=";PRO

```

IF PRO=3 THEN
YS=-.5*H: YF=CCY: MY=9
M=MY-1
DY=(YF-YS)/M
EY3=0: SY3=0
y=YS
FOR I=1 TO M
EY3=(.5*H+y)*SLOP+E1
SY3=K*((ABS(EY3)^SHE))*SGN(EY3)
WRITE #2,y,EY3,ENIII,ETYA,SY3,SNIII,FTY
PRINT y,EY3,ENIII,ETYA,SY3,SNIII,FTY
y=YS+(I+1)*DY
NEXT I
END IF

```

```

IF PRO=1 OR PRO=2 OR PRO=3 THEN
YS=CCY: YF=CTY: MY=9
IF E2<ETY THEN YF=.5*H
M=MY-1
DY=(YF-YS)/M
EY2=0: SY2=0
y=YS
FOR I=1 TO M
EY2=(.5*H+y)*SLOP+E1
SY2=ELM*EY2
WRITE #2,y,EY2,ENIII,ETYA,SY2,SNIII,FTY
PRINT y,EY2,ENIII,ETYA,SY2,SNIII,FTY
y=YS+(I+1)*DY
NEXT I
END IF

```

```

IF PRO=2 OR PRO=3 OR PRO=4 THEN
YS=CTY: YF=.5*H: MY=11
M=MY-1
DY=(YF-YS)/M
EP1=0: SP1=0
y=YS
FOR I=1 TO M
EP1=(.5*H+y)*SLOP+E1
SP1=K*((ABS(EP1)^SHE))*SGN(EP1)
WRITE #2,y,EP1,ENIII,ETYA,SP1,SNIII,FTY
PRINT y,EP1,ENIII,ETYA,SP1,SNIII,FTY
y=YS+(I+1)*DY
NEXT I
END IF

```

```

CLOSE #2
REM STOP
CLS
ETY=ETY0
ECY=ECY0
K=K0
SHE=SHE0
GOTO 10
SUB PrintScreen(scale%,x%,y%) STATIC
' CALCULATE ARRAY SIZE NEEDED TO GET ENTIRE
SCREEN

```

```

max&=((4+(SYSTEM(6)+1)*2*INT(SYSTEM(5)+16)/16))/4+1
IF max&>32767 OR max&*4+60>FRE(0) THEN
BEEP:EXIT SUB
  DIM pt%(1),screen&(max&) 'pt%() will contain 0,0
  LocalToGlobal pt%(0) 'Find window position on screen
  GET (-pt%(1), -pt%(0)) - (SYSTEM(5)-
pt%(1),SYSTEM(6)-pt%(0)),screen&
  ' "prompt" allows user to select an orientation so the dump
will
  ' fit on a page.

```

```

OPEN "LPT1:prompt" FOR OUTPUT AS #10

WINDOW OUTPUT #10
IF scale% THEN PUT(0,0)-(x%,y%), screen& ELSE
PUT(0,0),screen&
CLOSE #10
ERASE pt%,screen& 'release memory
END SUB

```

Figure 7 is a program printout sample of the cross-section characteristics derived from back-to-back strain gauge data.

```

ELASTIC MODULUS E=? 10500
YIELD STRESS Fty=? 38
MAX STRESS Ftu=? 58
STRAIN @ MAX STRESS Eyu=? .06
TENSION YIELD STRAIN 3.619048E - 03
STRAIN HARDENING EXPO. n= .1505829
STRENGTH COEF K= 88.59669
RECT BAR THICKNESS H=? 1.4
BAR WIDTH w=? .74
TEST MAX STRAIN E2=? .02
TEST MIN STRAIN E1=? -.01
TOTAL AXIAL LOAD N= 16.21604
AXIAL LOAD STRESS SN= 15.65255
AXIAL LOAD STRAIN EN= 1.490719E-03
MAX BENDING STRAIN EM= 1.850928E-02
BENDING NEUTRAL AXIS CM= -.1637665
BENDING MOMENT M= 17.29161
MOMENT / AXIAL LOAD RATIO R= 1.066328

```

Figure 7. Program sample output.

Figures 8 and 9 illustrate the strain and stress distributions along the element thickness using Cricket Graph III™ and figure 7 program input. Only solid lines are program plotted. Dashed lines, shades, and notes are superimposed to further illustrate routine patterns and significant characteristics.

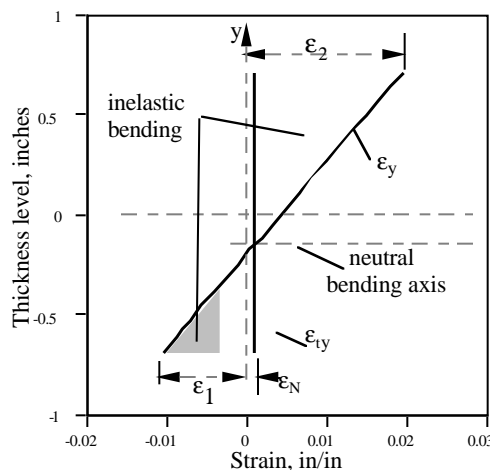


Figure 8. Strain distributions.

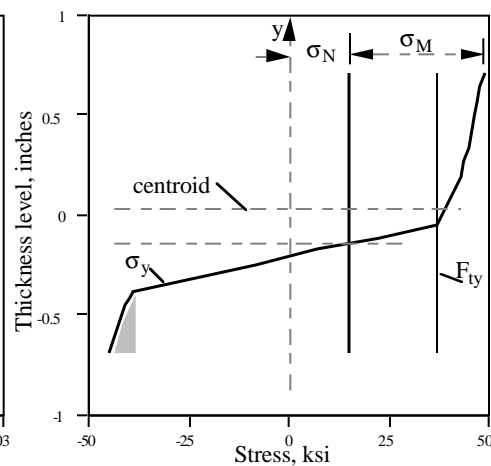


Figure 9. Stress distributions.

## V. CONCLUSIONS

Demand for ever-improving structural performance is driving design practices and manufacturing processes to new and innovative technologies whose ultimate success depends on the experimental verification of their performance and reliability. This study examined binding verification criteria and converged on a potential static test source for accepting submarginal structures for the wrong reason or prematurely failing sound ones.

Experimental verification consists of two coherent, deterministic static test parts. Structural response within the elastic limit is verified with a precisely specified external load representing maximum predicted operational environments. The ultimate factor of safety covers rare events in which no statistical design data exist and its traditional and historical usage exerts the greatest influence on design and acceptance criteria. However, the order-of-magnitude larger strains (and therefore displacements) imposed by the ultimate factor of safety may distort the applied load transmission.

A technique was developed to identify and assess verification load transfer discrepancy through back-to-back surface-mounted strain gauge data, which is applicable throughout the elastic and inelastic range of the structural material. The technique is reduced to a user-friendly program for convenience and expedience. The program is also applicable for monitoring structural response from field or flight tests environments.

It is concerning that verification test results often report surface strain measurements to conform very well with predicted math models up to the yield point, but then unexpectedly deviate during the inelastic loading to premature fracture. Reasons offered are usually indefinite. Perhaps this suggested technique may extend the basis for a more definite test evaluation.

## REFERENCES

1. Total Quality Management Executive Briefing, Marshall Space Flight Center, NASA, American Supplier Institute, Inc., Dearborn, MI, Version 1.1, 1991.
2. Dieter, G.: "Mechanical Metallurgy." Third edition, McGraw-Hill, Inc., NY, 1986.
3. Anon: "Structural Factor of Safety and Test Verification." NASA White paper, October 9, 1992.
4. Phillips, A.: "Introduction to Plasticity." The Ronald Press Company, 1956.
5. Verderaime, V.: "Plate and Butt-Weld Stresses Beyond Elastic limits." NASA TP-3075, January 1991.